Journal of Solid State Chemistry 184 (2011) 1939–1945

Contents lists available at ScienceDirect

Journal of Solid State Chemistry

journal homepage: www.elsevier.com/locate/jssc

Preparation and physical properties of antiperovskite-type compounds $CdNCo_{3-z}Ni_z$ $(0 \le z \le 3)$

Bing He [a,b,*], Cheng Dong [a], Lihong Yang [a], Linhui Ge [a], Hong Chen [a]

[a] National Laboratory for Superconductivity, Institute of Physics, Chinese Academy of Sciences, Beijing 100190, China
[b] Luzhou Medical College, Luzhou, Sichuan 646000, China

ARTICLE INFO

Article history:
Received 11 April 2011
Received in revised form
24 May 2011
Accepted 29 May 2011
Available online 12 June 2011

Keywords:
Nitride
Antiperovskite
Solid solution
Ferromagnetism

ABSTRACT

A series of $CdNCo_{3-z}Ni_z$ $(0 \le z \le 3)$ samples were prepared from CdO and metal powders under NH_3 atmosphere at 743 K. The structural and physical properties were investigated by means of X-ray powder diffraction, temperature dependent resistivity and magnetic measurements. X-ray powder diffraction results show that $CdNCo_3$ is a new ternary nitride with antiperovskite structure, and it can form a complete solid solution series with $CdNNi_3$. Both $CdNCo_3$ and $CdNNi_3$ samples show metallic temperature dependent resistivity and exhibit a Fermi liquid behavior below 50 K. All samples are ferromagnetic, and their coercivity and remanence decrease as the Ni content increases. The temperature dependence of the magnetization of the $CdNCo_{3-z}Ni_z$ samples can be well fitted to the combination of a Bloch term and a Curie–Weiss term. The $CdNCo_3$ sample is ferromagnet with coercivity of 240 Oe at room-temperature. In contrast to the paramagnetism previously reported, our $CdNNi_3$ sample exhibits very soft and weak ferromagnetism.

1. Introduction

Since the superconductivity of $MgCNi_3$ was discovered in 2001 [1], much attention has been paid to research on the antiperovskite compounds. Most antiperovskite compounds can be described by a general formula AXT_3, where A is a divalent or trivalent metal, X is C or N, and T is a transition metal element. Many investigations have been performed on the antiperovskite carbides $ACNi_3$ (A=Cd, Zn, Al, Ga, In, etc.). Among these materials, only $CdCNi_3$ demonstrates superconductivity with T_c=3.4 K [2]. $ZnCNi_3$ is a Pauli paramagnetic (PM) metal [3], while both $AlCNi_3$ and $GaCNi_3$ take on strongly exchange–enhanced PM behaviors [4,5]. $In_{0.95}CNi_3$ behaves as a ferromagnetic (FM) metal below the Curie temperature (577 K) [6]. Besides carbides, many antiperovskite nitrides have been studied. Fe-based nitrides $MNFe_3$ (M=Fe, Mn, Au, Ag, Sn, Pd, Ni, and Pt) exhibit interesting Invar-like behavior [7–15]. Mn-based nitrides $ANMn_3$ (A=Cu, Zn, Ga, Ge, etc.) show large negative thermal expansion triggered by antiferromagnetic (AFM) or FM transitions [16,17]. Recently several Ni-based nitrides, i.e., $ZnNNi_3$ [18], $InNNi_3$ [19] and $CdNNi_3$ [20] have been synthesized. $ZnNNi_3$ is the only known superconductor (T_c=3 K) at present among these Ni-based antiperovskite nitrides. $InNNi_3$ exhibits a spin–glass-like behavior, while $CdNNi_3$ is a PM metal. Based on these experimental facts, we can conclude that the physical properties of the antiperovskite compounds are quite diversified and fascinating, and they are very sensitive to their chemical compositions.

In order to systematically study the relationship between the chemical compositions and physical properties of the antiperovskites, it is necessary to synthesize new materials with the antiperovskite structure. In this paper, we report the synthesis and physical properties of a series of $CdNCo_{3-z}Ni_z$ $(0 \le z \le 3)$ samples.

2. Experimental

We prepared a series of $CdNCo_{3-z}Ni_z$ (z=0, 0.5, 1.0, 1.5, 2.0, 2.5, 3.0) samples by solid–gas reactions. CdO (> 99%), Co (99.7%) and Ni (99.5%) powders were used as starting materials. Extra 20% CdO was added in order to compensate evaporation during the reaction. The mixtures were thoroughly ground, and then put into alumina boats. The mixtures were heated in a tube furnace at 743 K for 8 h under static NH_3 atmosphere and subsequently furnace cooled to room temperature. During the heating process, fresh NH_3 gas was refilled five times to remove the H_2O vapor produced in the reaction. The obtained intermediate products are loose powders. To facilitate the resistivity and magnetic measurements, the intermediate products were then reground thoroughly, pressed into pellets and sintered for another 8 h under the same reaction conditions. In addition, compounds $CdNCo_{3-z}Ni_z$ can also be synthesized using the corresponding transition metal oxide as a precursor instead of metal powders.

* Corresponding author at: National Laboratory for Superconductivity, Institute of Physics, Chinese Academy of Sciences, Beijing 100190, China.
E-mail address: hebing@ssc.iphy.ac.cn (B. He).

0022-4596/$ - see front matter © 2011 Elsevier Inc. All rights reserved.
doi:10.1016/j.jssc.2011.05.051

The powder X-ray diffraction (XRD) data of the samples were collected on a MXP18A-HF diffractometer with Cu $K\alpha$ radiation at room temperature. The 2θ scan range was from 20° to 120° with a step size of 0.02° and a counting time of 3 s. The Rietveld refinement of the powder X-ray diffraction data was performed with the program RIETAN-2000 [21]. The grain morphology and microstructure were obtained using a field emission scanning electron microscope (FE–SEM, FEI XL 30 S-FEG) and the chemical compositions of samples were examined using an energy-dispersive X-ray spectroscopy (EDX) attachment. An Elementary Vario MICRO CUBE (Germany) elemental analyzer was employed to determine the nitrogen content.

The temperature dependence of electrical resistivity was measured using the four-probe method in the temperature range of 5–300 K. Magnetic measurements were performed employing a superconducting quantum interference device magnetometer (MPMS XL–7, Quantum Design) in the temperature range of 2–300 K.

3. Results and discussion

3.1. Nitrogen content and crystal structure

Fig. 1 shows the EDX spectra of CdN_yM_3 (M=Co, Ni) samples. According to the EDX analysis, the atomic ratios of Cd:Co in CdN_yCo_3 and Cd:Ni in CdN_yNi_3 are 1.0:2.94 and 1.0:2.95, respectively.

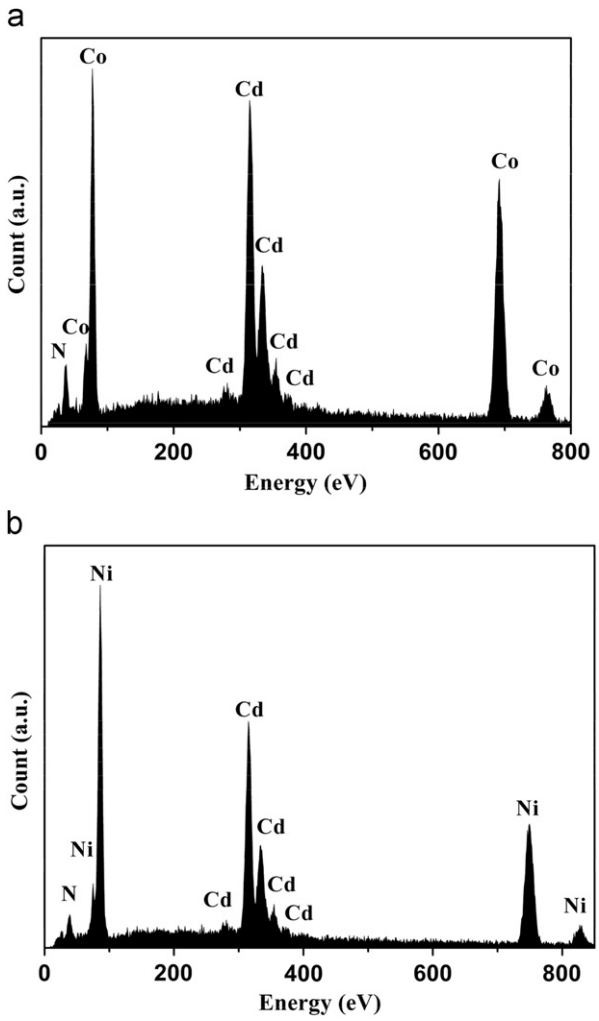

Fig. 1. EDX spectrum of $CdNCo_3$ (a) and $CdNNi_3$ (b).

The actual Cd:M ratios are in consistent with the ideal ratio (1:3) within the experimental error around 2%. Furthermore, no impurity phase was found in the powder XRD patterns of these samples. Fig. 2 shows the SEM images of the $CdN_yCo_{3-z}Ni_z$ samples. From Fig. 2, it can be seen that the particle sizes of the $CdN_yCo_{3-z}Ni_z$ samples are in the range of 50–150 nm, and some micron-sized aggregations exist in samples containing both nickel and cobalt.

The powder XRD patterns for CdN_yM_3 (M=Co, Ni) samples are shown in Fig. 3. The diffraction peaks could be well indexed to the antiperovskite structure. Using the antiperovskite structure as a starting model, the lattice parameters and nitrogen content y for both nitrides are refined using the Rietveld method. The refined structural parameters and the R factors are listed in Table 1. The refined lattice parameter (a=3.8419(5) Å) for CdN_yCo_3 is smaller than that of CdN_yNi_3 (a=3.8483 (3) Å). The elemental analysis shows that the prepared samples are stoichiometric within the experimental errors. The weight percentages of nitrogen for CdN_yCo_3 and CdN_yNi_3 are 4.6% and 4.5%, corresponding to the value of $y\sim1.0$ and 0.97, respectively. So the values of y in CdN_yCo_3 and CdN_yNi_3 samples were taken as 1.0 in the following discussions. The crystal structure of $CdNCo_3$ is shown in the inset of Fig. 3a.

Fig. 4 shows the XRD patterns for the series of $CdNCo_{3-z}Ni_z$ samples. The diffraction peaks shifted towards lower angle regions as the nickel content increases, suggesting that the effective radius of Ni are slightly larger than that of Co in the antiperovskites (Fig. 4b). As shown in Fig. 5, the lattice parameters of the $CdNCo_{3-z}Ni_z$ samples linearly increase from 3.8419(5) to 3.8483(3) Å as the nickel content z increases from 0 to 3, indicating that a complete solid solution series was formed between $CdNCo_3$ and $CdNNi_3$.

3.2. Electronic transport and magnetic properties

Fig. 6 shows the temperature dependence of the resistivity of the $CdNCo_3$ and $CdNNi_3$ samples. Both samples exhibit metallic behaviors over the measured temperature range (5–300 K) and no superconductivity is found down to 5 K. As can be seen in the inset of Fig. 6, below 50 K the resistivity can be fitted with the equation

$$\rho(T)=\rho_0+AT^2 \quad (1)$$

which is suggestive of a Fermi liquid behavior. $CdNCo_3$ has a larger residual resistivity ρ_0 (242.2 μ Ω cm) than that of $CdNNi_3$ (80.72(2) μ Ω cm). This probably reflects the stronger spin fluctuations [22,23] in $CdNCo_3$. At high temperatures (50–300 K), the resistivity of $CdNNi_3$ shows a linear behavior, which is attributable to the electron–phonon scattering.

Fig. 7 shows the temperature dependence of magnetization for $CdNCo_{3-z}Ni_z$ samples obtained in zero-field-cooled (ZFC) and field-cooled (FC) modes. There are two common features in their magnetization versus temperature curves. The first one is the divergence of the FC and ZFC curves, and the second one is that all ZFC curves exhibit a broad cusp at low temperatures (25.1–60.5 K). The irreversibility temperature (T_{irr}), where the ZFC and FC curves diverge, shift to the lower temperature with the increase of applied field. From Fig. 7a and c, we can see clearly that T_{irr} decreases as the applied field increases for $CdNCo_3$ and $CdNNi_3$ samples. The $CdNCo_{3-z}Ni_z$ (z=0.5, 1.0, 1.5, 2.5) samples show much higher irreversibility, as evidenced by significant splitting of the ZFC and FC curves at or near room temperature (Fig. 7b). Similar behavior is seen in frozen ferrofluids [24] and assemblies of nanoparticles [25]. The crystallite size of our samples are in the range of 50–150 nm, so this bifurcation in ZFC and FC curves can be attributed to the presence of strong interactions between nanosized magnetic particles [26]. As shown

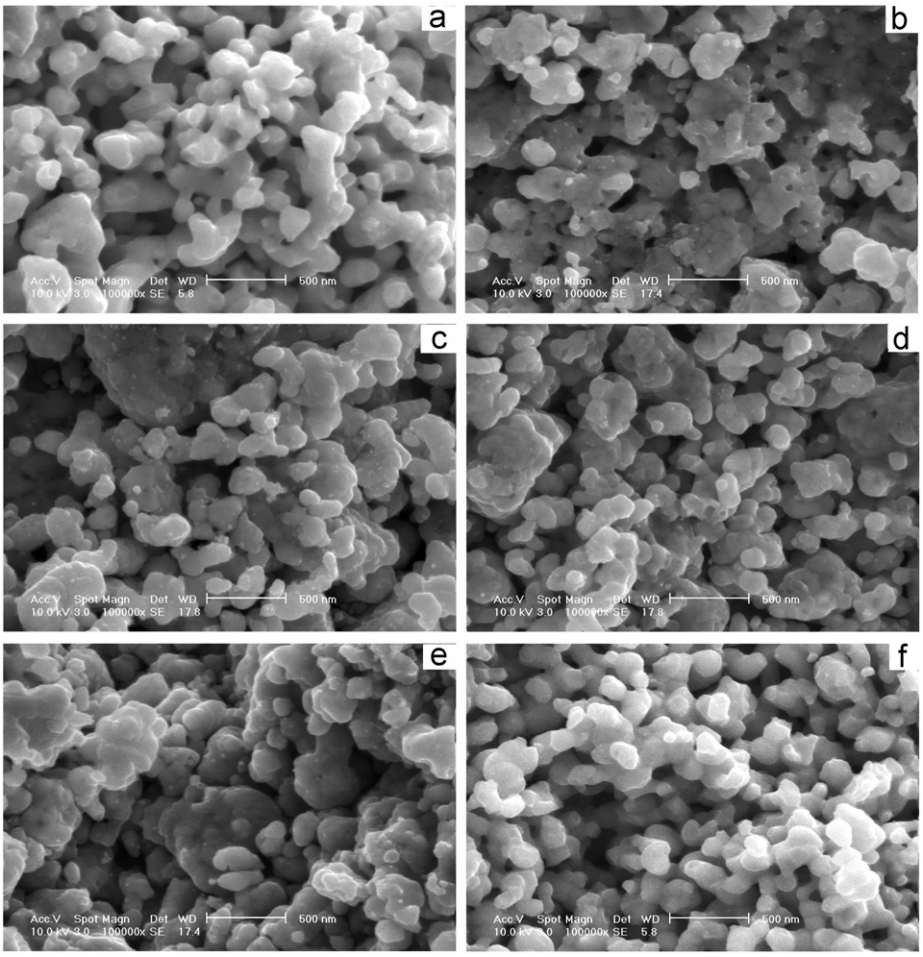

Fig. 2. SEM micrographs of the $CdNCo_{3-z}Ni_z$ samples: $z=0$ (a), $z=0.5$ (b), $z=1.0$ (c), $z=1.5$ (d), $z=2.5$ (e), and $z=3.0$ (f).

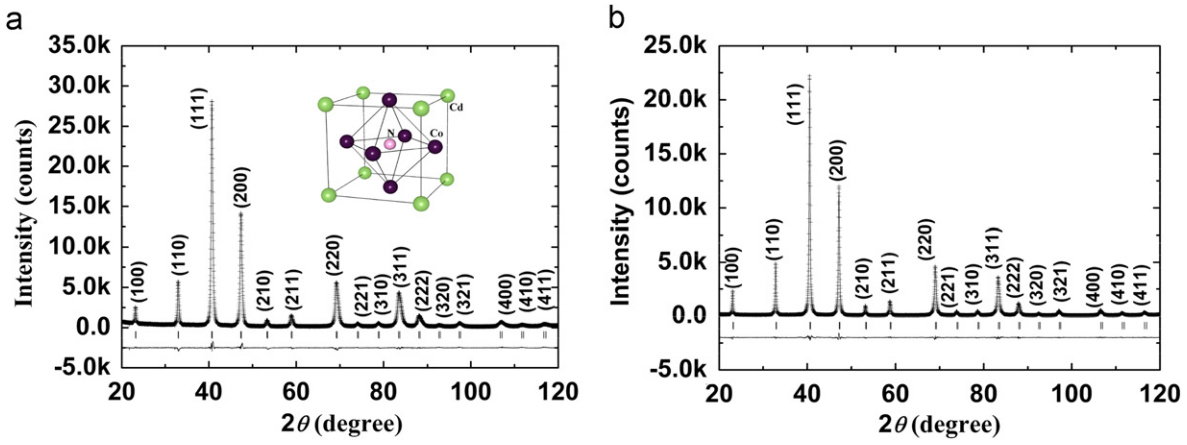

Fig. 3. XRD diffraction patterns (plus marks) and Rietveld refinement results (solid curve) for $CdNCo_3$ (a) and $CdNNi_3$ (b). The curves at the bottom of each figure represent the difference between the observed and calculated patterns. The short vertical lines mark the positions of allowed reflections. Inset: crystal structure of $CdNCo_3$.

in Fig. 7a and c, the ZFC curves of both $CdNCo_3$ and $CdNNi_3$ samples show broad cusps at applied field of 50 Oe, and the cusps occur at temperature (T_f) around 27 and 60 K for $CdNCo_3$ and $CdNNi_3$, respectively. With the increase of applied field from 50 to 1 k Oe, the T_f of $CdNNi_3$ shifts toward lower temperature and the cusp for $CdNCo_3$ disappears at 500 Oe. The broad cusp (T_f) in ZFC curve can be attributed to the superparamagnetic blocking of spins [27,28]. The superparamagnetic blocking process is the competition between thermal and anisotropy energies of the particles. It is clear that as the applied field increases, the anisotropy energy of the particles decreases. When this happens, the particles need less thermal energy to cross over the energy barrier and thus the T_f decreases. Simultaneously, the extent of irreversibility tends to vanish as the external field increases.

Fig. 8 plots the isothermal M (H) curves for the $CdNCo_{3-z}Ni_z$ ($z=0$, 1.0, and 3.0) samples at different temperatures (10, 150 and 300 K). The insets of Fig. 8 show the hysteresis loops for the samples. From the hysteresis loops, we can see clearly that the

Table 1
Refined structural parameters for $CdNCo_3$ (a) and (b) $CdNNi_3$.

Atom	Site	x	y	z	B (Å^2)	Occupancy
(a) R_p =6.23%, R_{wp}=4.33%, R_{ex}=3.86%, a=3.8419(5) Å						
Cd	1*a*	0	0	0	1.31(7)	1.0
N	1*b*	0.5	0.5	0.5	1.0(1)	1.0
Co	3*c*	0	0.5	0.5	1.24(7)	1.0
(b) R_p=4.32%, R_{wp}=6.77%, R_{ex}=5.46%, a=3.8483(3) Å						
Cd	1*a*	0	0	0	1.12(8)	1.0
N	1*b*	0.5	0.5	0.5	1.6(2)	1.0
Ni	3*c*	0	0.5	0.5	1.13(7)	1.0

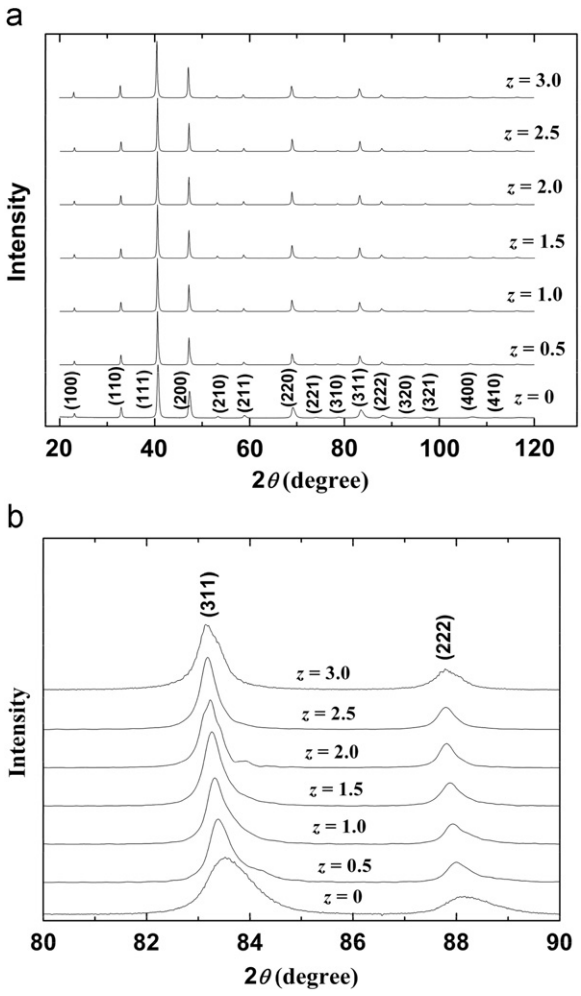

Fig. 4. (a) XRD patterns for the series of $CdNCo_{3-z}Ni_z$ samples. (b) The enlarged portion of the reflections (3 1 1) and (2 2 2).

coercivity and remanence of the samples decrease as the Ni content increases. At room temperature, the coercivity of $CdNCo_3$ (240 Oe) is notably higher than that of $CdNNiCo_2$ (190 Oe). $CdNNi_3$ has very small coercivity and remanence above 150 K, since its hysteresis loops (inset of Fig. 8c) are hardly visible.

The Arrott plot technique was also used in order to determine the magnetic properties of the $CdNCo_{3-z}Ni_z$ samples. Fig. 9 shows the Arrott plot for $CdNCo_{3-z}Ni_z$ (z=0, 1.0, and 3.0) samples. The Arrott plot (M^2 against H/M) provides a useful criterion for the magnetic property, because a positive (negative) intercept on the ordinate of the extrapolated linear behavior in the high field portion corresponds to the ferromagnetic (paramagnetic) state. The intercepts are positive (Fig. 9a and b) for both $CdNCo_3$

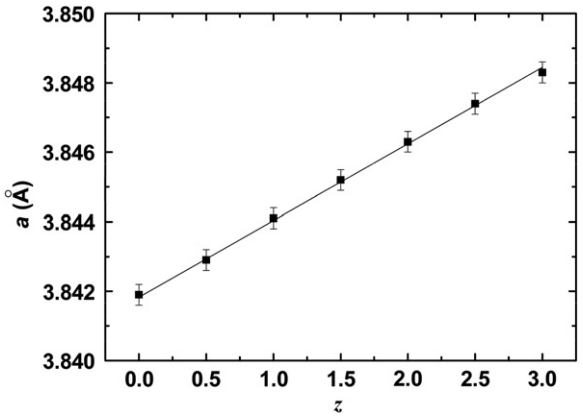

Fig. 5. Variation of lattice parameter a with composition of $CdNCo_{3-z}Ni_z$ samples. The solid line represents linear fit.

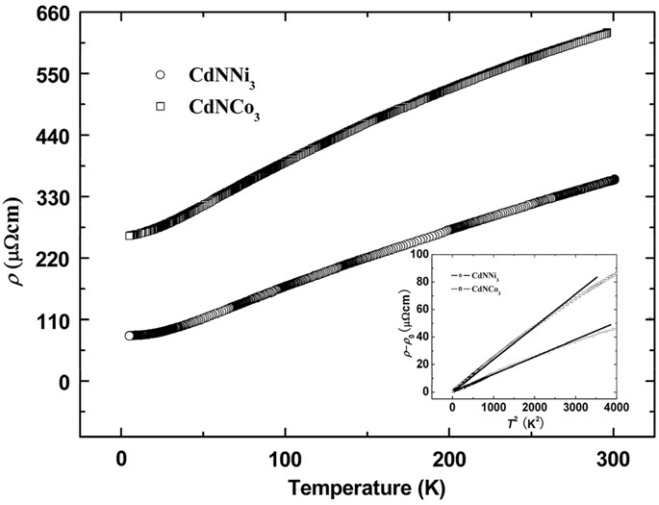

Fig. 6. Temperature-dependent resistivity of $CdNCo_3$ and $CdNNi_3$. Inset: linear fitting of $\rho(T)-\rho_0$ vs T^2 below 50 K.

and $CdNNiCo_2$ samples, so they are obviously ferromagnetic. The intercepts for the $CdNNi_3$ sample (Fig. 9c) are very close to the origin of coordinate. Nonetheless, they are positive. So, our $CdNNi_3$ sample has very weak ferromagnetism. This result is different from the earlier report [20]. This difference indicates that the physical properties of $CdNNi_3$ sample are very sensitive to the synthesis routes and variation in compositions.

Fig. 10 depicts the temperature dependence of the magnetization for $CdNCo_{3-z}Ni_z$ (z=0, 0.5, 1.0, 1.5, 2.5, and 3.0) samples at a magnetic field of 50 Oe. The $M(T)$ curves of the $CdNCo_{3-z}Ni_z$ (z=0, 2.5, and 3.0) samples can be well fitted by using a combination of a Bloch law and a Curie–Weiss behavior [29–31]. The solid curves in Fig. 10 show the fitting results using the following equation:

$$M(T) = M_0[1 + B_0T^{3/2} + B_1T^{5/2}] + C/(T-\theta) \quad (2)$$

where B_0 and B_1 are spin wave parameters, because the spins are polarized to form spin–wave interactions in ferromagnetic region. The Curie–Weiss behavior has been observed in interacting ferrofluids, where θ is a measure of the interaction strength [32–34]. However, the $M(T)$ curves of $CdNCo_{3-z}Ni_z$ (z=0.5, 1.0, and 1.5) samples require only the $T^{3/2}$ and the $T^{5/2}$ terms for a satisfactory fit, and the Curie–Weiss contribution can be ignored. Because the Curie–Weiss contribution mainly comes from the interactions between the nanosized particles, and such interactions might be reduced in samples with micron-sized aggregations. The fitted

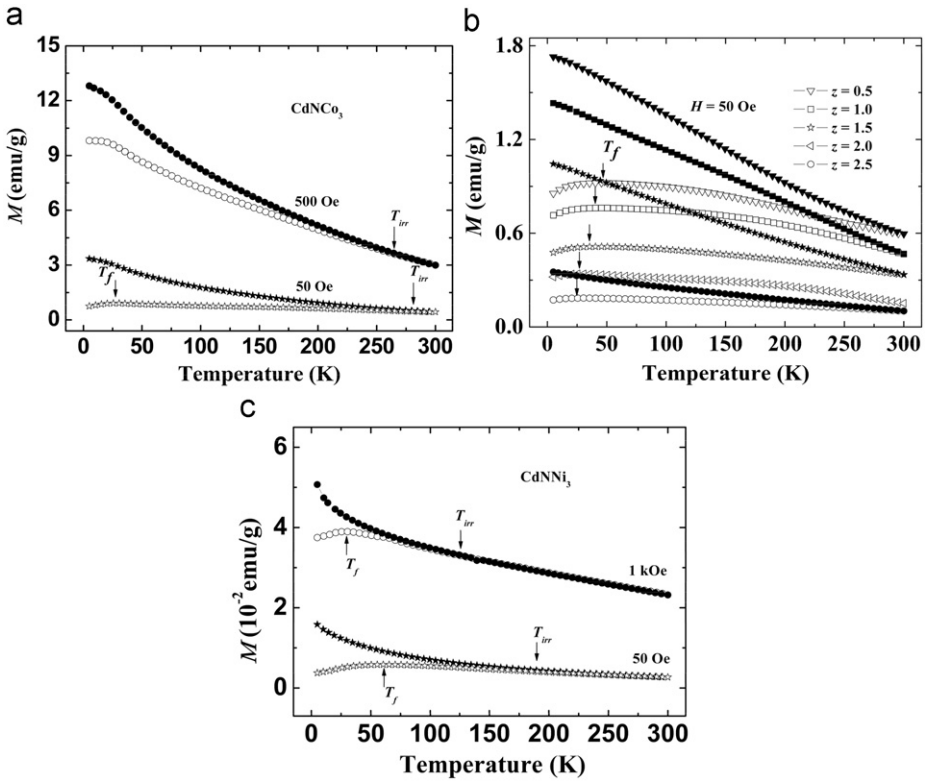

Fig. 7. Temperature dependence of the ZFC (open symbols) and FC (filled symbols) dc magnetization curves: $CdNCo_3$ (a), $CdNCo_{3-z}Ni_z$ (b), $CdNNi_3$ (c). Arrow symbols indicate T_{irr} and T_f, respectively.

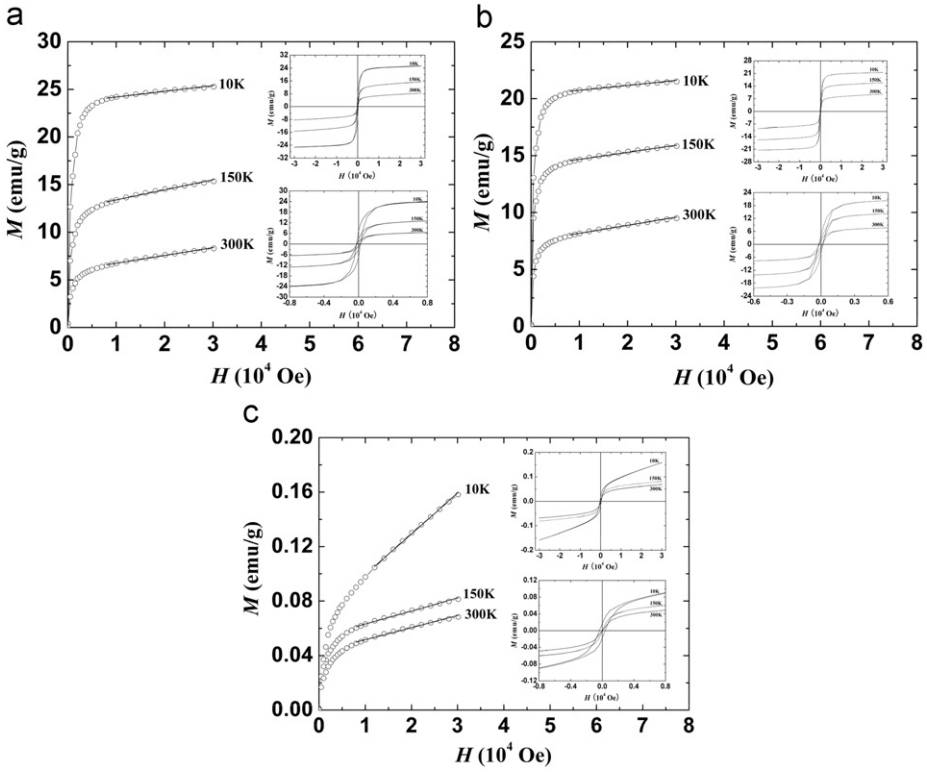

Fig. 8. Magnetization vs magnetic field isotherm (M–H) curves at different temperatures: $CdNCo_3$ (a), $CdNNiCo_2$ (b), $CdNNi_3$ (c). Solid lines represent the linear fit. The inset shows the hysteresis loops (up) and details of the hysteresis loops at low fields (down).

parameters and the goodness of fit (R^2) are listed in Table 2. As can be seen in Table 2, the values of θ are negative. The negative value for θ may be attributed to the antiferromagnetic ordering of the nanosized ferromagnetic particles when they aggregate. The changing trend of the M_0 values indicates that the effective magnetic moment per atom decreases when the nickel content increases in this system.

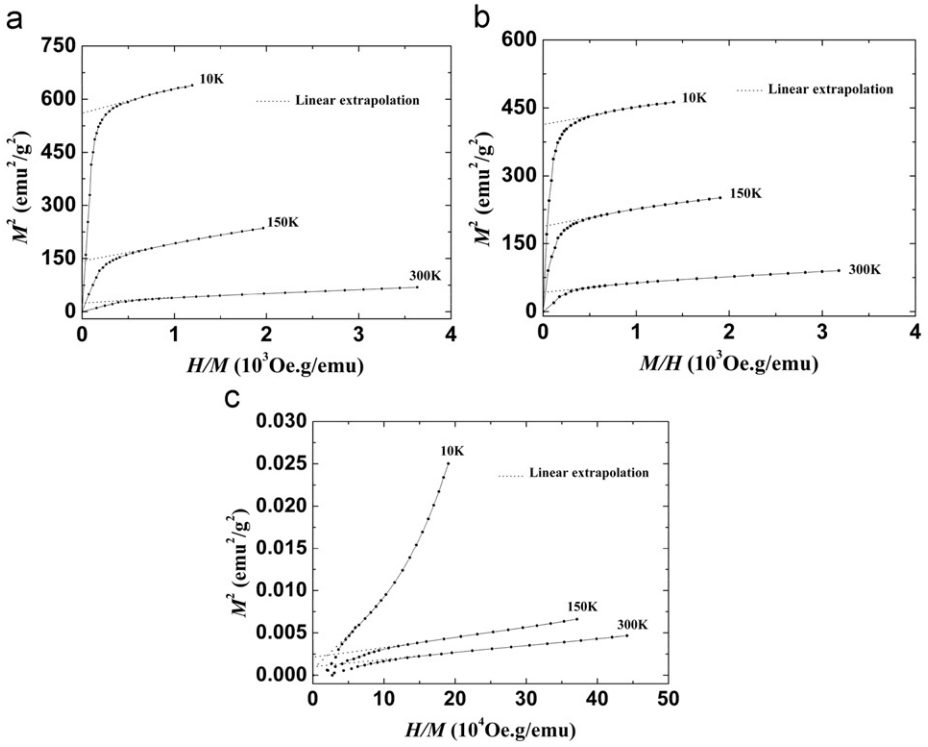

Fig. 9. Arrott plots (M^2–H/M) at different temperatures: $CdNCo_3$ (a), $CdNNiCo_2$ (b), and $CdNNi_3$ (c).

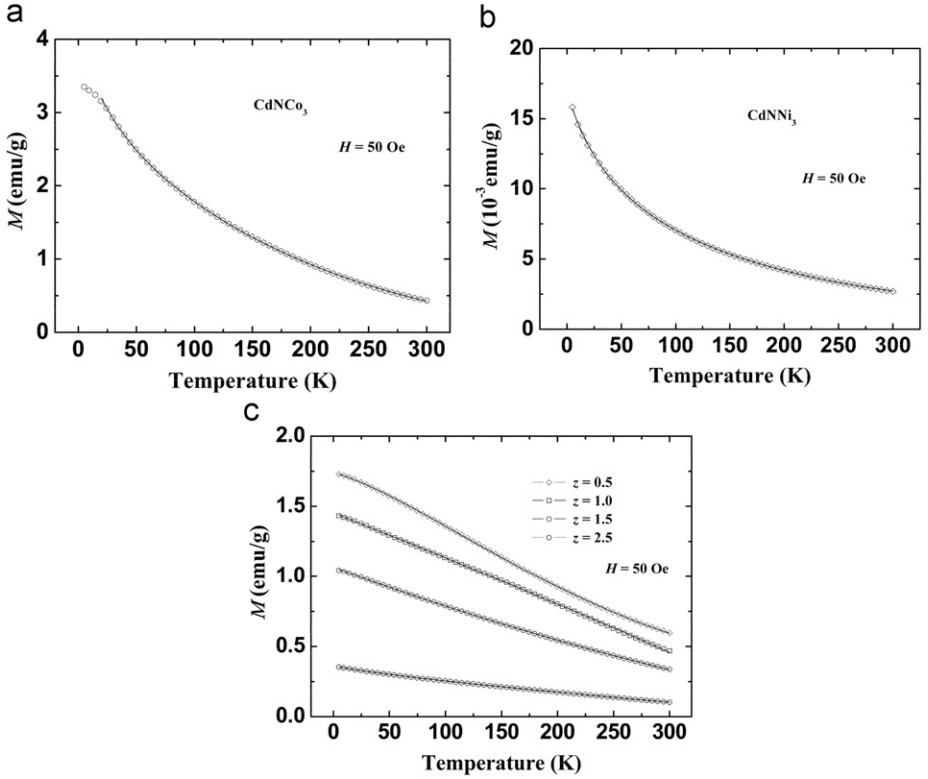

Fig. 10. Temperature dependence of the magnetization at a magnetic field of 50 Oe: $CdNCo_3$ (a), $CdNNi_3$ (b), $CdNCo_{3-z}Ni_z$ (c). The solid line represents the fit to Eq. (2).

4. Conclusion

In summary, the structure, magnetic and electronic transport properties of the $CdNCo_{3-z}Ni_z$ samples have been investigated. The new ternary nitride $CdNCo_3$ has the typical antiperovskite structure (space group $Pm3m$, lattice parameter 3.8419(5) Å). The resistivity of $CdNCo_3$ and $CdNNi_3$ show quadratic temperature dependence below 50 K. $CdNCo_3$ and $CdNNi_3$ can form a complete solid solution series. Both $CdNCo_3$ and $CdNNiCo_2$ samples exhibit ferromagnetism below 300 K. $CdNNi_3$ has a soft and weak ferromagnetism below 300 K,

Table 2
Results of $CdNCo_{3-z}Ni_z$ samples fit to Eq. (2).

sample	M_0 (emu/g)	B_0 ($K^{-3/2}$)	B_1 ($K^{-5/2}$)	C (emu K/g)	θ (K)	R^2
$z=0$	2.02	-4.62×10^{-3}	4.95×10^{-6}	81	−40	0.99997
$z=0.5$	1.98	-3.36×10^{-3}	3.39×10^{-6}	–	–	0.99994
$z=1.0$	1.45	-2.83×10^{-3}	1.87×10^{-6}	–	–	0.99991
$z=1.5$	1.06	-2.78×10^{-3}	1.57×10^{-6}	–	–	0.99997
$z=2.5$	0.297	-2.49×10^{-3}	4.58×10^{-7}	5.4	−86	0.99998
$z=3.0$	4.30×10^{-3}	-4.21×10^{-3}	4.65×10^{-6}	0.66	−52	0.99992

which is different from literature report. The temperature dependence of the magnetization of $CdNCo_3$ and $CdNNi_3$ can be well fitted using a combination of a Bloch law and a Curie–Weiss behavior. The Curie–Weiss behavior here is mainly comes from the interactions between nanosized particles, and the ferromagnetism is dominating in samples with larger crystallite sizes. Therefore, the magnetic properties of the samples are sensitive to the crystallite size distributions.

Acknowledgments

We are grateful to Prof. Jirong Sun for helpful discussions. This work was supported by the National Natural Science Foundation of China (No. 20871119) and National Basic Research Program of China (973 Program) 2011CBA00100 and 2011CB808202.

Appendix A. Supplementary materials

Supplementary materials associated with this article can be found in the online version at doi:10.1016/j.jssc.2011.05.051.

References

[1] T. He, Q. Huang, A.P. Ramirez, Y. Wang, K.A. Regan, N. Rogado, M.A. Hayward, M.K. Haas, J.S. Slusky, K. Inumara, Nature (London) 411 (2001) 54.
[2] M. Uehara, T. Amano, S. Takano, T. Kori, T. Yamazaki, Y. Kimishima, Physica C 440 (2006) 6.
[3] M.S. Park, J. Giim, S.H. Park, Y.W. Lee, S.I. Lee, E.J. Choi, Supercond. Sci. Technol. 17 (2004) 274.
[4] P. Tong, Y.P. Sun, X.B. Zhu, W.H. Song, Phys. Rev. B 74 (2006) 224416.
[5] P. Tong, Y.P. Sun, X.B. Zhu, W.H. Song, Phys. Rev. B 73 (2006) 245106.
[6] P. Tong, Y.P. Sun, X.B. Zhu, W.H. Song, Solid State Commun. 141 (2007) 33.
[7] S.F. Matar, P. Mohn, G. Demazeau, B. Siberchicot, J. Phys. 49 (1988) 1761 (Paris).
[8] S.F. Matar, G. Demazeau, B. Siberchicot, IEEE Trans. Magn. 26 (1990) 60.
[9] C. Cordier-Robert, J. Foct, Eur. J. Solid State Inorg. Chem. 29 (1992) 39.
[10] P. Mohn, K. Schwarz, S.F. Matar, G. Demazeau, Phys. Rev. B 45 (1992) 4000.
[11] C.A. Kuhnen, R.S. de Figueiredo, V. Drago, E.Z. da Silva, J. Magn. Magn. Mater. 111 (1992) 95.
[12] C.A. Kuhnen, A.V. dos Santos, Solid State Commun. 85 (1993) 273.
[13] C.A. Kuhnen, A.V. dos Santos, J. Magn. Magn. Mater. 130 (1994) 353.
[14] S. Suzuki, H. Sakamoto, J. Minegismi, V. Omote, IEEE Trans. Magn. 17 (1981) 3017.
[15] S.F. Matar, G. Demazeau, P. Hagenmuller, J.G.M. Armitage, P.C. Riedi, Eur. J. Solid State Inorg. Chem. 26 (1989) 517.
[16] D. Fruchart, E.F. Bertaut, J. Phys. Soc. Jpn. 44 (1978) 781.
[17] K. Takenaka, H. Takagi, Appl. Phys. Lett. 87 (2005) 261902.
[18] M. Uehara, A. Uehara, K. Kozawa, Y. Kimishima, J. Phys. Soc. Jpn. 78 (2009) 033702.
[19] W.H. Cao, B. He, C.Z. Liao, L.H. Yang, L.M. Zeng, C. Dong, J. Solid State Chem. 182 (2009) 3353.
[20] M. Uehara, A. Uehara, K. Kozawa, Y. Kimishima, Physica C 470 (2010) S688.
[21] F. Izumi, T. Ikeda, Mater. Sci. Forum. 189 (2000) 321.
[22] N.V. Baranov, A.A. Yermakov, A. Podlesnyak, J. Phys.: Condens. Matter. 15 (2003) 5371.
[23] J.R. Jeffries, N.A. Frederick, E.D. Bauer, H. Kimura, V.S. Zapf, K.D. Hof, T.A. Sayles, M.B. Maple, Phys. Rev. B 72 (2005) 024551.
[24] Weili Luo, S.R. Nagel, T.F. Rosenbaum, R.E. Rosensweig, Phys. Rev. Lett. 67 (1991) 2721.
[25] K. O'Grady, M. El–Hilo, R.W. Chantrell, IEEE Trans. Magn. 29 (1993) 2608.
[26] J. Cieślak, B.F.O. Costa, S.M. Dubiel, M. Reissner, W. Steiner, J. Phys.: Condens. Matter 17 (2005) 2985.
[27] B.H. Sohn, R.E. Cohen, G.C. Papaefthyrniou, J. Magn. Magn. Mater. 182 (1998) 216.
[28] L. Zhang, G.C. Papaefthymiou, J.Y. Ying, J. Phys. Chem. B 105 (2001) 7414.
[29] L. Yue, R. Sabiryanov, E.M. Kirkpatrick, D.L.L. Pelecky, Phys. Rev. B 62 (2000) 8969.
[30] F.J. Dyson, Phys. Rev. 102 (1956) 1217.
[31] R. Pauthenet, J. Appl. Phys. 53 (1982) 2029.
[32] M. Holmes, K. O'Grady, J. Popplewell, J. Magn. Magn. Mater. 85 (1990) 47.
[33] F. Söffge, E. Schmidbauer, J. Magn. Magn. Mater. 24 (1981) 54.
[34] V.M. Dubovik, M.A. Martsenyuk, N.M. Martsenyuk, J. Magn. Magn. Mater. 150 (1995) 105.